New Journal of Physics
The open access journal for physics

Large momentum-dependence of the main dispersion 'kink' in the high-T_c superconductor $Bi_2Sr_2CaCu_2O_{8+\delta}$

N C Plumb[1,5,6], T J Reber[1], H Iwasawa[2], Y Cao[1], M Arita[2], K Shimada[2], H Namatame[2], M Taniguchi[2], Y Yoshida[3], H Eisaki[3], Y Aiura[3] and D S Dessau[1,4,6]

[1] Department of Physics, University of Colorado, Boulder, CO 80309-0390, USA
[2] Hiroshima Synchrotron Radiation Center, Hiroshima University, Higashi-Hiroshima 739-0046, Japan
[3] National Institute of Advanced Industrial Science and Technology, Tsukuba, Ibaraki 305-8568, Japan
[4] JILA, University of Colorado and NIST, Boulder, CO 80309-0440, USA
E-mail: nicholas.plumb@psi.ch and daniel.dessau@colorado.edu

New Journal of Physics **15** (2013) 113004 (13pp)
Received 24 April 2013
Published 1 November 2013
Online at http://www.njp.org/
doi:10.1088/1367-2630/15/11/113004

Abstract. Ultrahigh resolution angle-resolved photoemission spectroscopy with low-energy photons is used to study the detailed momentum dependence of the well-known nodal 'kink' dispersion anomaly of $Bi_2Sr_2CaCu_2O_{8+\delta}$. We find that the kink's location transitions smoothly from a maximum binding energy of about 65 meV at the node of the d-wave superconducting gap to 55 meV roughly one-third of the way to the antinode. Meanwhile, the self-energy spectrum corresponding to the kink dramatically sharpens and intensifies beyond a critical point in momentum space. We discuss the possible bosonic spectrum in energy and momentum space that can couple to the k-space dispersion of the electronic kinks.

[5] Present address: Swiss Light Source, Paul Scherrer Institut, CH-5232 Villigen PSI, Switzerland.
[6] Authors to whom any correspondence should be addressed.

Contents

1. Introduction **2**
2. Analysis and results **2**
2.1. Experimental 2
2.2. Momentum-dependent self-energy 3
2.3. Scattering $\boldsymbol{q}$-space analysis of the kink momentum dependence 5
3. Discussion **8**
Acknowledgments **10**
References **10**

1. Introduction

One of the defining characteristics of the electronic structure of the high-T_c cuprates is the presence of an especially prominent anomaly, or 'kink', in the electronic dispersion, which corresponds to a strong feature in the complex electronic self-energy spectrum $\Sigma(\boldsymbol{k}, \omega) = \Sigma'(\boldsymbol{k}, \omega) + i\Sigma''(\boldsymbol{k}, \omega)$. The origin of the kink—whether it is due to interactions of the electrons with bosons (particularly phonons [1, 2] or magnetic excitations [3–5]) or some other phenomenon [6]—is still heavily debated. Likewise the kink's connection to superconductivity, and whether the interactions it signifies may either form or break Cooper pairs, or be altogether irrelevant, remains unknown.

At the nodes of the d-wave superconducting gap, this kink appears at a binding energy of roughly 60–70 meV [7–10]. Meanwhile near the antinode, a seemingly stronger kink is located at about 20–40 meV, depending on doping [11–13]. While a possible connection between the nodal and antinodal kinks remains a mystery, the new data here fills in details of the evolving physics between these points. Such information is crucial for obtaining a complete understanding of the behaviour and origin of the kink and hence the electron–boson coupling in the high-T_c superconductors.

2. Analysis and results

2.1. Experimental

The data presented here were obtained from $Bi_2Sr_2CaCu_2O_{8+\delta}$ (Bi2212) near optimal doping with $T_c \approx 89$ K. Rotational alignment of the sample better than 1° was performed by Laue diffraction. The data were collected in the superconducting state at 10 K using a photon energy of 7 eV. Compared to conventional photon energies, the low photon energy greatly improves the photoelectron escape depth, momentum resolution and overall spectral sharpness [14]. Total combined energy resolution of the light source and analyser was about 7 meV. Angle-resolved photoemission spectroscopy (ARPES) cuts were taken along the (π, π) direction of the Fermi surface (FS).

2.2. Momentum-dependent self-energy

In the present work, we are especially concerned with the self-energy contribution due to electrons coupling to a collective mode over a sharp energy range, and we wish to isolate this from other interactions with smooth energy dependences (e.g. electron–electron scattering [15]). This is accomplished by assuming a smooth (in this case linear) *effective* bare band $\epsilon_{\rm eff}(\boldsymbol{k})$ for each ARPES cut that connects points on the dispersion far from the main kink. The real part of the effective self-energy is then simply

$$\Sigma'_{\rm eff}(\omega) = \omega - v_{\rm F}^{\rm eff}[k_m(\omega) - k_{\rm F}], \tag{1}$$

where $k_m(\omega)$ is the measured dispersion, $v_{\rm F}^{\rm eff}$ is the slope of $\epsilon_{\rm eff}(k)$ and $k_{\rm F}$ is the Fermi momentum. $\Sigma''_{\rm eff}(\omega)$ is then the Kramers–Kronig transformation of $\Sigma'_{\rm eff}(\omega)$. Unlike $\Sigma'(\omega)$, $\Sigma'_{\rm eff}(\omega)$ is well-behaved at its endpoints (by construction), and its Kramers–Kronig transformation is easily computed. Our routine sets the in-gap points of $\Sigma'_{\rm eff}(\omega)$ to zero and computes the transformation by fast Fourier transform assuming electron–hole symmetry. We have verified by simulations that a possible violation of electron–hole symmetry [16] should not significantly alter the findings here. We note that equation (1) is a conventional definition of $\Sigma'_{\rm eff}$. Recently it was shown that this definition undervalues the 'true' bosonic part of the self-energy by an overall scaling factor related to the coupling strength of electron–electron interactions, $\lambda_{\rm el-el}$ [17]. As this factor influences the magnitude of the self-energy, not its distribution along ω or $\boldsymbol{k}$, neglecting it will not affect the conclusions of the present study. A systematic assessment of $\lambda_{\rm el-el}$ in Bi2212, and hence the correct scaling factor to be applied to $\Sigma'_{\rm eff}$, is currently underway.

Figure 1(a) shows ARPES data collected along the FS in the first quadrant of the Brillouin zone. The colour scale represents the measured intensity 10 meV below $E_{\rm F}$. The thick solid lines in figure 1(a) are sketches of the antibonding (AB) and bonding band (BB) FSs based on a tight-binding model [18]. For 7 eV photons, only the AB is detected [19], which greatly simplifies the analysis. Two representative raw data cuts, corresponding to FS angles $\theta = 0.9^\circ$ and 16.3°, are indicated by the red curves labelled (i) and (ii), respectively. The spectra from these cuts are shown in figure 1(b). The dispersions from momentum distribution curve (MDC) fits are overlaid on the spectra (solid black curves). The dashed red lines are assumed effective bare bands used to calculate corresponding effective self-energy spectra $\Sigma_{\rm eff}(\omega)$ at each θ. These effective bare bands are determined by linear fits from -230 to -200 meV that are constrained to pass through the MDC peak location at $\omega = -\Delta(\theta)$ (i.e. $k_{\rm F}$).

Figure 1(c) shows the Lorentzian MDC widths for each cut from (i) to (ii), while figure 1(d) depicts $\Sigma'_{\rm eff}(\omega)$ (black, right axis) and $\Sigma''_{\rm eff}(\omega)$ (red, left axis) for cuts (i) and (ii). The full spectrum of $\Sigma'_{\rm eff}(\theta, \omega)$ is plotted as a colour scale in figure 1(e). We define the kink energy $\Omega_{\rm kink}$ as the location of the peak in $\Sigma'_{\rm eff}(\omega)$ at each θ. These values are determined by quadratic fits over a range ± 20 meV about the maximum of each spectrum. The error bars show the standard deviations ($\pm\sigma$) returned from the fits. Figure 1(f) depicts $-\partial\Sigma''_{\rm eff}/\partial\omega$ as a function of ω and θ. To reduce noise in the derivative, some light smoothing was applied to the $\Sigma'_{\rm eff}$ spectrum. Together panels (e)–(f) highlight the evolution of the self-energy over the nodal region, which exhibits both dispersive behaviour and sharpening. The results are fully consistent with the behaviour of the MDC widths in panel (c) and the electronic dispersion anomalies in (b), providing an important verification of the self-consistency of the data and analysis methods. It is worth noting that the quantity $-\partial\Sigma''_{\rm eff}/\partial\omega$ in panel (f) is somewhat related to a useful parameter of strong coupling theory—the Eliashberg boson coupling spectrum $\alpha^2F(\boldsymbol{k}, \nu)$, where ν is the energy axis for bosons. In an *ungapped* system at $T = 0$, $\Sigma''(\boldsymbol{k}, \omega) = \pi \int_0^{|\omega|} {\rm d}\nu\alpha^2F(\boldsymbol{k}, \nu)$ [20],

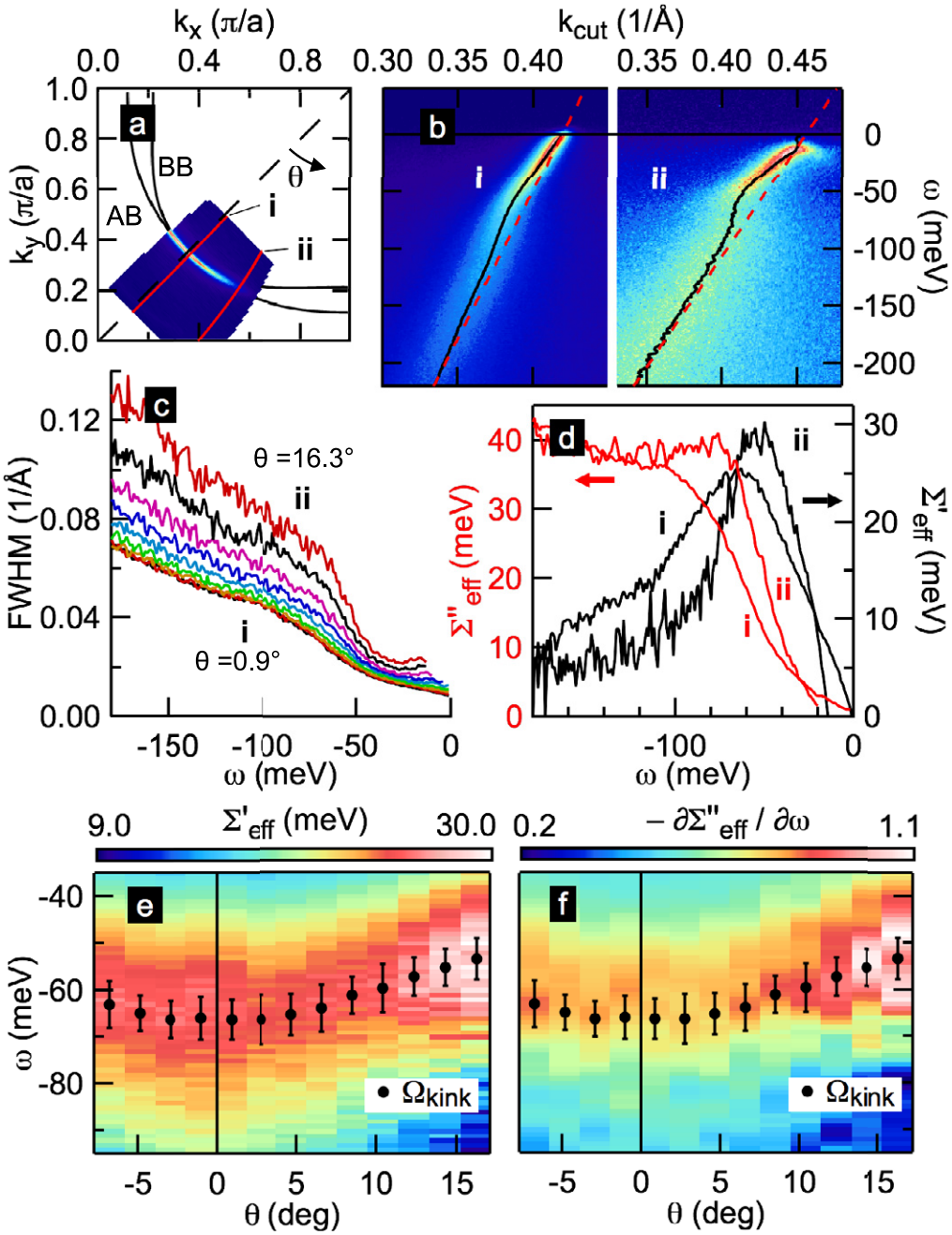

Figure 1. (a) First quadrant of the FS of Bi2212. The colour scale is the measured spectral intensity 10 meV below E_F. Two representative cuts (i) and (ii) are indicated by red curves. The black curves are sketches of the AB and BB sheets. The use of 7 eV photons isolates the antibonding band. (b) Raw ARPES data from cuts (i) and (ii). The solid black curves are the peak positions of the fitted MDCs, while the dashed red lines are the effective noninteracting bands for the dispersions (see text). (c) MDC widths at cuts progressing away from the node. (d) Real (black) and imaginary (red) components of the effective electronic self-energy for cuts (i) and (ii). (e) $\Sigma'_{\rm eff}$ and (f) $-\partial\Sigma''_{\rm eff}/\partial\omega$ as a function of θ and ω. The black dots are the peak locations of $\Sigma'_{\rm eff}$ at each θ, which we call $\Omega_{\rm kink}(\theta)$.

although the anisotropic gapping in cuprates can significantly alter this relationship. Addressing this issue via suitable 'gap referencing' is a key objective of the present work.

Two key points are evident from figure 1. Firstly, $\Omega_{\rm kink}$ evolves smoothly as a function of θ in the nodal region, shifting towards $E_{\rm F}$ by about 10 meV from $\theta = 0$ to 15°. Secondly, the nature of $\Sigma_{\rm eff}$ appears to change abruptly past a critical point in $\boldsymbol{k}$-space. While by eye the kink perhaps becomes more dramatic going from node to antinode [21], this fact alone does not necessarily mean that the self-energy strengthens, since Σ is related to the bare band velocity, which decreases away from the node. Indeed, the results in figures 1(c)–(f) show that over much of the near-nodal region $\Sigma_{\rm eff}(\omega)$ is relatively unchanged, despite the visual appearance that the kink is 'getting stronger'. However, for $\theta \gtrsim 10°$ figure 1(e) shows a rapid increase in the peak of $\Sigma'_{\rm eff}(\omega)$. This corresponds with sharpening of the step in $\Sigma''_{\rm eff}(\omega)$ seen in figure 1(f). The findings in figure 1 contrast with a previous study of overdoped Pb-Bi2212 where it was argued that the scattering rate near $E_{\rm F}$ is independent of $\boldsymbol{k}$ [22]. We also point out that these results contradict recent claims that the energy $\Omega_{\rm kink}$ is constant near the node and then suddenly jumps at a 'crossover' point on the FS $\sim 15°$ away from the node [23, 24], though there still may be a crossover parameterized by, e.g. the intensity and sharpness of the features in $\Sigma_{\rm eff}(\omega, \theta)$, as seen in figures 1(e) and (f).

2.3. Scattering $\boldsymbol{q}$-space analysis of the kink momentum dependence

The large nodal ARPES kink seen in cuprates is generally explained as the result of the coupling of the electrons to a bosonic mode of energy $\Omega_{\rm boson}$. In particular, $\Omega_{\rm kink}$ may be able to tell us which electrons interact with which bosons, and in principle this can yield information about which (or even whether) bosons act as the 'glue' responsible for the formation of the Cooper pairs. The new finding of the large, smooth dispersion of $\Omega_{\rm kink}(\boldsymbol{k})$ is therefore an important result that may connect directly to the coupling mechanism of the electrons within a pair. Here we consider how to best connect the k-dispersion of the kink to known data of the q-space dependence of various bosonic modes.

In the simplest picture, the kink energies $\Omega_{\rm kink}$ will be exactly those of the coupling boson [8], though this ignores the 'gap referencing' which is simple for an s-wave superconductor ($|\Omega_{\rm kink}| = \Omega_{\rm boson} + \Delta$) but more complicated for a d-wave superconductor in which Δ is strongly k-dependent. In the presence of an anisotropic gap $\Delta(\boldsymbol{k})$, a bosonic mode with energy $\Omega_{\rm boson}(\boldsymbol{q})$ scattering an electron purely from $\boldsymbol{k}$ to $\boldsymbol{k}'$ is expected to produce an ARPES dispersion kink below $E_{\rm F}$ at [25]

$$|\Omega_{\rm kink}(\boldsymbol{k})| = \Omega_{\rm boson}(\boldsymbol{q}) + \Delta(\boldsymbol{k}') \tag{2}$$

which can be deduced by considering the set of photoholes at $\boldsymbol{k}$ that can be annihilated via electrons decaying from $\boldsymbol{k}'$ and emitting bosons $\Omega_{\rm boson}(\boldsymbol{q})$. An argument along these lines (but for an isotropic gap) is presented in section 7.3 of [20]. We will make use of this gap referencing relationship throughout the present work in order to identify the boson dispersions appropriate to particular scattering scenarios. Additional corrections for relating $\Omega_{\rm kink}$ to $\Omega_{\rm boson}$ are believed to be too small to account for the dispersive behaviour of $\Omega_{\rm kink}(\boldsymbol{k})$ [26] and therefore should not qualitatively alter the present work.

There is reason to believe that the predominant electron–boson scattering relevant to the nodal kink falls along some symmetry direction, thus simplifying the connection between k- and q-space. For instance, SF observed by inelastic neutron scattering (INS) are peaked

at points on or near the $(\xi, \xi, 0)$ line [29–31]. Likewise, both experiment [32] and theory [1, 33] suggest the Cu–O 'half-breathing' phonon mode scatters electrons primarily along $(\xi, 0, 0)$ (equivalently $(0, \xi, 0)$), and there is evidence that this mode couples strongly to electrons [34] and, in particular, may contribute to the nodal kink [19].

In the case of phonons, numerical calculations find that, on the whole, the scattering matrix elements are fairly complicated [1, 33]. Nevertheless, they are expected to evolve smoothly over the FS and exhibit some preference for particular directionalities. Thus, despite the complexity of the full scattering problem, one can reasonably expect to find *qualitative* agreement between the actual phonon dispersion and the inference from ARPES—at least over a limited portion of the FS.

To proceed with our analysis, assumed scattering $\boldsymbol{q}$'s along symmetry directions are illustrated in figure 2(a). We consider cases where electrons may scatter horizontally, vertically, or diagonally via inter- or intra-hole-pocket vectors. The kink energies obtained in figure 1(e) are plotted in figure 2(b) as a function of FS angle θ (red ■). The blue circles (●) are the corresponding gap-referenced boson energies Ω^*_{boson}. The asterisk (*) denotes that only the special cases of scattering vectors shown in that panel apply. Under these circumstances, $\Delta(\boldsymbol{k}) = \Delta(\mathbf{k}')$, leading to

$$\Omega^*_{\text{boson}}(\theta) = |\Omega_{\text{kink}}(\theta)| + \Delta(\theta). \tag{3}$$

In calculating $\Omega^*_{\text{boson}}(\theta)$, we used $\Delta(\theta)$ based on our ARPES-measured values, which were found to have excellent agreement with the expected d-wave form, with maximum (antinodal) magnitude $\Delta_0 = 30\,\text{meV}$. The gap measurements shown here were performed using the newly developed tomographic density of states technique [35, 36], and we have checked that the analysis and results that follow are essentially unchanged if the symmetrized energy distribution curve method is employed [37].

The extracted $\boldsymbol{q}$-space dispersions of Ω_{kink} and Ω^*_{boson} under these various scattering scenarios are shown in figures 2(c)–(f). The insets in each of these panels illustrate how the q values on each horizontal axis were determined. For simplicity and generalizability of the analysis, we consider each scattering channel independently. For an assumed bosonic mode that would scatter electrons in the $(\xi, 0, 0)/(0, \xi, 0)$ directions, a given $\boldsymbol{k}$ point on the FS could couple via two orthogonal vectors—one shorter than the node–node distance in $\boldsymbol{q}$-space ($\xi \sim 0.35$) and the other longer (labelled 'H/V short' and 'H/V long' in figures 2(c) and (d), respectively). However, in general these short and long $\boldsymbol{q}$ channels would not be expected to contribute equally to the appearance of the kink, but rather their relative scattering intensities would evolve around the FS (only matching at the node–node distance, where they have the same length). To disentangle these paired interactions, the $\Omega_{\text{kink}}(\boldsymbol{q})$ and $\Omega^*_{\text{boson}}(\boldsymbol{q})$ curves were extracted by treating the short and long scattering vectors separately, as plotted in figures 2(c) and (d). This is a logical choice, since one or the other (either the short or long vector) would probably be more influential at any given point on the FS. Meanwhile, the diagonal intra- and inter-hole-pocket vectors ('Intra' and 'Inter' in figures 2(e) and (f) respectively) are also treated independently, since they are distinct in how they couple the topology of the FS.

In figures 2(c)–(f), the extracted $\Omega^*_{\text{boson}}(\boldsymbol{q})$ curves (blue ●) are compared to various Cu–O phonon dispersions in $YBa_2Cu_3O_{6+x}$ (YBCO) with $x = 0$ ($\bigtriangledown$) and $x = 1$ ($\bigtriangleup$) [27], as well as two phonon branches observed in $Bi_2Sr_{1.6}La_{0.4}Cu_2O_{6+\delta}$ (Bi2201, $\diamondsuit$) [23]. Additionally, a sketch of the dispersion of a high-energy branch of incommensurate SF is shown in figure 2(f) (green shaded line).

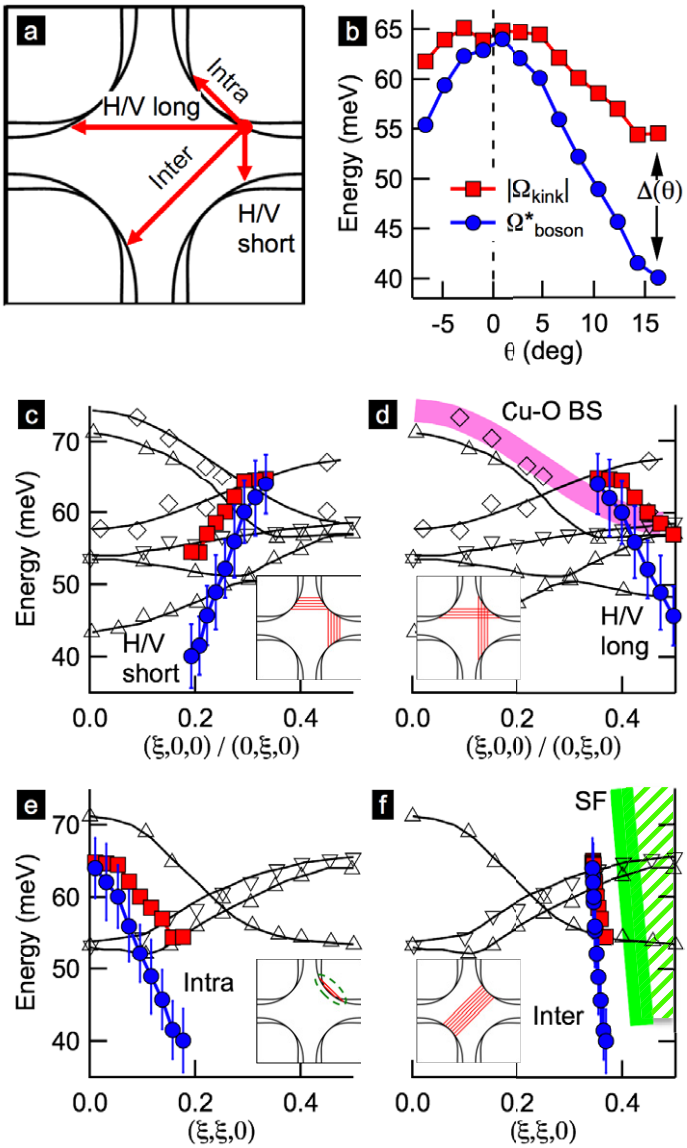

Figure 2. Extracting the boson coupling mode dispersion assuming the following scattering $\boldsymbol{q}$ directionalities in (a) horizontal and vertical (H/V), intra-hole-pocket (Intra) and inter-hole-pocket (Inter). (b) $|\Omega_{\text{kink}}|$ and Ω^*_{boson} as a function of FS angle θ. Ω^*_{boson} (equation (3)) is the boson energy for the special cases of scattering along symmetry directions such that $\Delta(\boldsymbol{k}') = \Delta(\boldsymbol{k})$, as depicted in (a). (c), (d) Dispersions of $|\Omega_{\text{kink}}(\boldsymbol{q})|$ (red ■) and $\Omega^*_{\text{boson}}(\boldsymbol{q})$ (blue ●), assuming that scattering occurs horizontally/vertically in the Brillouin zone. Curves for $|\Omega_{\text{kink}}(\boldsymbol{q})|$ and $\Omega^*_{\text{boson}}(\boldsymbol{q})$ have been extracted considering the short (c) and long (d) H/V scattering channels separately. The extracted dispersions are compared to those of Cu–O phonons measured by INS in $YBa_2Cu_3O_7$ (△) and $YBa_2Cu_3O_6$ (▽) [27], as well as phonons observed by IXS in Bi2201 (◇) [23]. The pink highlighted Cu–O bond-stretching (Cu–O BS) branch, in particular, has been identified by some previous experiments as possibly relevant to the nodal kink. (e), (f) Analogous plots assuming diagonal intra- and inter-pocket scattering.

Figure 2. (Continued) The green shaded line in (f) is the approximate dispersion of the high-energy branch of spin fluctuations (SF) observed in optimally doped Bi2212 [28]. The hatched area indicates that this region is observed in the neutron data to be somewhat filled in by the width of the dispersion peaks. For simplicity, error bars from figures 1(e) and (f) are shown only for the $\Omega^*_{\text{boson}}(\boldsymbol{q})$ curve in each panel.

Overall, the extracted $\Omega^*_{\text{boson}}(\boldsymbol{q})$ curves do not provide clear support that the kink primarily originates from electron–phonon interactions, although the data may not be wholly inconsistent with this possibility. For instance, in figure 2(d), there is a limited $\boldsymbol{q}$-space region ($\boldsymbol{q} \approx$ (0.3–0.4,0,0)) where the extracted boson dispersion roughly overlaps with the Cu–O bond stretching phonon branch, as pointed out in [23]. However, for larger values of $\boldsymbol{q}$ extending toward (0.5, 0, 0), $\Omega^*_{\text{boson}}(\boldsymbol{q})$ diverges from the Cu–O bond stretching phonon branch with a different slope. In this regard, our data show greater overall similarity between $\Omega^*_{\text{boson}}(\boldsymbol{q})$ and the SF dispersion in figure 2(f), which differ by merely a simple offset in ω and/or $\boldsymbol{q}$, perhaps reflecting systematic differences between the techniques and/or samples used in the studies. The rough correspondence between the kink and the SF dispersion compares favorably with spectral analysis of the spin response function extracted from ARPES data by Chatterjee *et al* [38], though their formalism only considered SF and did not provide a comparison to phonon dispersions. Moreover, that approach treated the spectral function holistically, rather than isolating the kink feature and considering its explicit connection to the bosonic spectral function.

The SF dispersion in figure 2(f) is the high-energy branch of incommensurate spin excitations so far observed in many cuprates [28–31, 39]. It converges with a low-energy branch near ∼40 meV, where there is a well-known $\boldsymbol{q} = (0.5, 0.5)$-centred 'resonance' peak in the spin susceptibility at low T [40–43]. The effective self-energy obtained from our analysis intensifies significantly at Ω^*_{boson} somewhat near the resonance energy. This is depicted in figure 3, where the peak height of Σ'_{eff} (red triangles) is plotted versus Ω^*_{boson}. INS data from optimally doped Bi2212 (open circles) show the difference in scattered neutron intensity from 100 to 10 K, illustrating the location of the resonance [43]. Notably, within the context of an orbital-overlap model, coupling to the Cu–O bond-stretching phonon suggested by figure 2(d) is not expected to intensify in this manner at θ corresponding to Ω^*_{boson} close to the resonance [44]. With that said, the data is again only in rough agreement with the SF picture, and other studies imply that the strength of Σ'_{eff} is monotonic around the FS [45], meaning that it would not obey the peak-shaped trend of the INS data reproduced in figure 3. However, this does not fully undermine the possibility that the kink is SF-related, as it could instead signal a contribution to Σ'_{eff} at low energies (i.e. near the antinode) from additional types of electron–boson interactions, as we will discuss.

3. Discussion

The above analysis has relied on the key assumption of a dominant scattering mode and directionality, which, while consistent with interpretations of some INS and inelastic x-ray scattering (IXS) data and calculations, is not exhaustive. A natural potential counter example

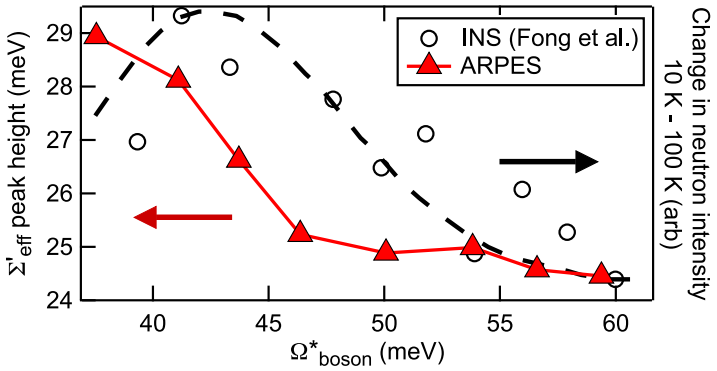

Figure 3. Peak height of $\Sigma'_{\rm eff}$ as a function of $\Omega^*_{\rm boson}$. The results are compared to INS data [43] highlighting the magnetic resonance at ~ 40 meV. The INS data points are the neutron scattering intensity at 100 K subtracted from the signal at 10 K.

is the case where all points on the FS couple primarily to the van Hove singularities at the antinodes—a situation in which the results would not be directly comparable with conventional INS/IXS data, since the $\boldsymbol{q}$'s would no longer fall along a straight line. Perhaps the best that can be said is that coupling strictly to the antinodes would shift the $\Omega_{\rm kink}(\boldsymbol{q})$ dispersion down universally by $\Delta_0 \approx 30$ meV such that $\Omega_{\rm boson}(\boldsymbol{q})$ would span an energy range of roughly 25–35 meV. These energies are home to many phonons in the cuprates [46], which in principle could combine their effects in some intricate way to produce the observed kink behaviour. A strong antinodal coupling appears unlikely, however, because this scenario would imply a huge shift of the nodal kink energy between the normal and superconducting states and/or as a function of doping. Multiple ARPES studies find no evidence of such a shift [10, 12, 21, 25, 47], although one case where the kink was interpreted to be composed of multiple phonon mode couplings arguably shows evidence of node–antinode scattering [48].

Reviewing the results, the analysis of $\Omega^*_{\rm boson}(\boldsymbol{q})$ for 'long' $(\xi, 0, 0)/(0, \xi, 0)$ scattering vectors found some region of agreement with the dispersion of a Cu–O bond stretching phonon (figure 2(d)), although the trends diverge as ξ extends out to 0.5. On the other hand, $\Omega^*_{\rm boson}(\boldsymbol{q})$ extracted for diagonal inter-hole-pocket scattering is similar to the dispersion of SF (figure 2(f)), merely differing by a simple offset in energy and/or $\boldsymbol{q}$. Additionally, figure 3 illustrates that the strength of the self-energy associated with the kink, plotted with respect to $\Omega^*_{\rm boson}$, has a qualitative resemblance to SF, and this is contrary to the behaviour predicted for electron–phonon coupling [44]. However, to the extent the data might be viewed as favouring the spin fluctuation picture, it poses an intriguing apparent paradox. A very detailed low-$h\nu$ ARPES study found an isotope shift in the energy of the nodal kink [19], giving strong merit to the phonon scenario. One possible explanation for this conflict is that electron–phonon interactions might constitute a finite but relatively small contribution to the total self-energy [49]. Alternatively, the results may signal a role for coupling between spin and lattice degrees of freedom [50–52].

The discovery of the large momentum dependence of the main nodal kink adds to the richness of strong electron–boson coupling phenomena in cuprates. It was recently shown that a newly discovered ultra-low-energy kink $\sim$10 meV below $E_{\rm F}$ [25, 53–55] has its own distinct momentum dependence that runs counter to the behaviour of the deeper-energy kink studied

here [56]. Specifically, unlike the larger main kink 65–55 meV below E_F, which evolves towards lower binding energy while moving from node to antinode, the ultra-low-energy kink closely follows the contour of the superconducting gap in the nodal region, moving to higher binding energy approaching the antinode. A natural, but spectroscopically demanding, next course of study will be to investigate the possible convergence of these two energy scales near the antinodal point and to see whether either or both this these connect with the antinodal feature observed near 20–40 meV, which historically has been regarded as a separate kink. Hence the data here, in concert with [56], open the possibility that interactions with distinct physical origins could combine within a narrow energy range in the antinodal region—perhaps with major implications for high-T_c superconductivity.

In conclusion, using low photon energy ARPES, we have mapped the detailed momentum dependence of the primary kink in the nodal k-space region of near-optimal Bi2212. From a simplifying treatment of the data that takes into account effects of the d-wave superconducting gap, the kink's dispersion seems inconsistent with most phonons, though over a limited range of momentum transfer ($\boldsymbol{q} \approx$ (0.3–0.4,0,0)) it bears some semblance to scattering due to a Cu–O bond-stretching mode. However, in terms of the momentum dependence of the location and sharpness/intensity of the self-energy feature, the greatest similarity is found with the dispersion of the upper branch of incommensurate SF.

Acknowledgments

Funding was provided by the DOE under project number DE-FG02-03ER46066. Experiments were conducted at BL-9A of the Hiroshima Synchrotron Radiation Center and BL5-4 of the Stanford Synchrotron Radiation Lightsource (SSRL). SSRL is operated by the DOE, Office of Basic Energy Sciences. We thank D Reznik, T P Devereaux and S Johnston for valuable conversations.

Note added. During review of this manuscript, a related article was published [57].

References

[1] Devereaux T P, Cuk T, Shen Z-X and Nagaosa N 2004 Anisotropic electron–phonon interaction in the cuprates *Phys. Rev. Lett.* **93** 117004

[2] Ruiz H S and Badía-Majós A 2009 Nature of the nodal kink in angle-resolved photoemission spectra of cuprate superconductors *Phys. Rev.* B **79** 054528

[3] Manske D, Eremin I and Bennemann K H 2001 Analysis of the elementary excitations in high-T_c cuprates: explanation of the new energy scale observed by angle-resolved photoemission spectroscopy *Phys. Rev. Lett.* **87** 177005

[4] Inosov D S *et al* 2007 Relation between the one-particle spectral function and dynamic spin susceptibility of superconducting $Bi_2Sr_2CaCu_2O_{8-\delta}$ *Phys. Rev.* B **75** 172505

[5] Dahm T, Hinkov V, Borisenko S V, Kordyuk A A, Zabolotnyy V B, Fink J, Buchner B, Scalapino D J, Hanke W and Keimer B 2009 Strength of the spin-fluctuation-mediated pairing interaction in a high-temperature superconductor *Nature Phys.* **5** 217–21

[6] Byczuk K, Kollar M, Held K, Yang Y-F, Nekrasov I A, Pruschke Th and Vollhardt D 2007 Kinks in the dispersion of strongly correlated electrons *Nature Phys.* **3** 168–71

[7] Bogdanov P V *et al* 2000 Evidence for an energy scale for quasiparticle dispersion in $Bi_2Sr_2CaCu_2O_8$ *Phys. Rev. Lett.* **85** 2581–4

[8] Lanzara A *et al* 2001 Evidence for ubiquitous strong electron–phonon coupling in high-temperature superconductors *Nature* **412** 510–4
[9] Kaminski A, Randeria M, Campuzano J C, Norman M R, Fretwell H, Mesot J, Sato T, Takahashi T and Kadowaki K 2001 Renormalization of spectral line shape and dispersion below T_c in $Bi_2Sr_2CaCu_2O_{8+\delta}$ *Phys. Rev. Lett.* **86** 1070–3
[10] Johnson P D *et al* 2001 Doping and temperature dependence of the mass enhancement observed in the cuprate $Bi_2Sr_2CaCu_2O_{8+\delta}$ *Phys. Rev. Lett.* **87** 177007
[11] Campuzano J C *et al* 1999 Electronic spectra and their relation to the (π, π) collective mode in high-T_c superconductors *Phys. Rev. Lett.* **83** 3709–12
[12] Gromko A D, Fedorov A V, Chuang Y-D, Koralek J D, Aiura Y, Yamaguchi Y, Oka K, Ando Y and Dessau D S 2003 Mass-renormalized electronic excitations at $(\pi, 0)$ in the superconducting state of $Bi_2Sr_2CaCu_2O_{8+\delta}$ *Phys. Rev.* B **68** 174520
[13] Cuk T *et al* 2004 Coupling of the B_{1g} phonon to the antinodal electronic states of $Bi_2Sr_2Ca_{0.92}Y_{0.08}Cu_2O_{8+\delta}$ *Phys. Rev. Lett.* **93** 117003
[14] Koralek J D *et al* 2006 Laser based angle-resolved photoemission, the sudden approximation and quasiparticle-like spectral peaks in $Bi_2Sr_2CaCu_2O_{8+\delta}$ *Phys. Rev. Lett.* **96** 017005
[15] Ingle N J C *et al* 2005 Quantitative analysis of Sr_2RuO_4 angle-resolved photoemission spectra: many-body interactions in a model Fermi liquid *Phys. Rev.* B **72** 205114
[16] Hashimoto M *et al* 2010 Particle–hole symmetry breaking in the pseudogap state of Bi2201 *Nature Phys.* **6** 414–8
[17] Iwasawa H, Yoshida Y, Hase I, Shimada K, Namatame H, Taniguchi M and Aiura Y 2013 'True' bosonic coupling strength in strongly correlated superconductors *Sci. Rep.* **3** 1930
[18] Markiewicz R S 2004 Bridging k and q space in the cuprates: comparing angle-resolved photoemission and STM results *Phys. Rev.* B **69** 214517
[19] Iwasawa H *et al* 2008 Isotopic fingerprint of electron–phonon coupling in high-T_c cuprates *Phys. Rev. Lett.* **101** 157005
[20] Mahan G D 2000 *Many-Particle Physics* 3rd edn (New York: Plenum)
[21] Sato T *et al* 2003 Observation of band renormalization effects in hole-doped high-T_c superconductors *Phys. Rev. Lett.* **91** 157003
[22] Bogdanov P V, Lanzara A, Zhou X J, Yang W L, Eisaki H, Hussain Z and Shen Z X 2002 Anomalous momentum dependence of the quasiparticle scattering rate in overdoped $Bi_2Sr_2CaCu_2O_8$ *Phys. Rev. Lett.* **89** 167002
[23] Graf J, d'Astuto M, Jozwiak C, Garcia D R, Saini N L, Krisch M, Ikeuchi K, Baron A Q R, Eisaki H and Lanzara A 2008 Bond stretching phonon softening and kinks in the angle-resolved photoemission spectra of optimally doped $Bi_2Sr_{1.6}La_{0.4}Cu_2O_{6+\delta}$ superconductors *Phys. Rev. Lett.* **100** 227002
[24] Garcia D R, Graf J, Jozwiak C, Hwang C G, Eisaki H and Lanzara A 2010 Crossover region between nodal and antinodal states at the Fermi level of optimally doped and overdoped $Bi_2Sr_{1.6}Nd_{0.4}CuO_{6+\delta}$ *Phys. Rev.* B **81** 184527
[25] Plumb N C, Reber T J, Koralek J D, Sun Z, Douglas J F, Aiura Y, Oka K, Eisaki H and Dessau D S 2010 Low-energy (<10 meV) feature in the nodal electron self-energy and strong temperature dependence of the Fermi velocity in $Bi_2Sr_2CaCu_2O_{8+\delta}$ *Phys. Rev. Lett.* **105** 046402
[26] Schachinger E and Carbotte J P 2009 Energy of the bosonic kinks in the quasiparticle spectrum of cuprate superconductors *Phys. Rev.* B **80** 094521
[27] Reichardt W 1996 Cu-O bond-stretching vibrations in $YBa_2Cu_3O_7$ studied by inelastic neutron scattering *J. Low. Temp. Phys.* **105** 807–12
[28] Xu G, Gu G D, Hucker M, Fauque B, Perring T G, Regnault L P and Tranquada J M 2009 Testing the itinerancy of spin dynamics in superconducting $Bi_2Sr_2CaCu_2O_{8+\delta}$ *Nature Phys.* **5** 642–6
[29] Pailhès S, Sidis Y, Bourges P, Hinkov V, Ivanov A, Ulrich C, Regnault L P and Keimer B 2004 Resonant magnetic excitations at high energy in superconducting $YBa_2Cu_3O_{6.85}$ *Phys. Rev. Lett.* **93** 167001

[30] Hayden S M, Mook H A, Dai P, Perring T G and Dogan F 2004 The structure of the high-energy spin excitations in a high-transition-temperature superconductor *Nature* **429** 531–4
[31] Tranquada J M *et al* 2004 Quantum magnetic excitations from stripes in copper oxide superconductors *Nature* **429** 534–8
[32] Reznik D 2010 Giant electron–phonon anomaly in doped La_2CuO_4 and other cuprates *Adv. Condens. Matter Phys.* **2010** 523549
[33] Giustino F, Cohen M L and Louie S G 2008 Small phonon contribution to the photoemission kink in the copper oxide superconductors *Nature* **452** 975–8
[34] Pintschovius L 2005 Electron–phonon coupling effects explored by inelastic neutron scattering *Phys. Status Solidi* b **242** 30–50
[35] Reber T J *et al* 2012 The origin and non-quasiparticle nature of Fermi arcs in $Bi_2Sr_2CaCu_2O_{8+\delta}$ *Nature Phys.* **8** 606–10
[36] Reber T J *et al* 2013 Prepairing and the 'filling' gap in the cuprates from the tomographic density of states *Phys. Rev.* B **87** 060506
[37] Norman M R, Randeria M, Ding H and Campuzano J C 1998 Phenomenology of the low-energy spectral function in high-T_c superconductors *Phys. Rev.* B **57** R11093–6
[38] Chatterjee U *et al* 2007 Dynamic spin-response function of the high-temperature $Bi_2Sr_2CaCu_2O_{8+\delta}$ superconductor from angle-resolved photoemission spectra *Phys. Rev.* B **75** 172504
[39] Reznik D, Bourges P, Pintschovius L, Endoh Y, Sidis Y, Masui T and Tajima S 2004 Dispersion of magnetic excitations in optimally doped superconducting $YBa_2Cu_3O_6$.95 *Phys. Rev. Lett.* **93** 207003
[40] Rossat-Mignod J, Regnault L P, Vettier C, Bourges P, Burlet P, Bossy J, Henry J Y and Lapertot G 1991 Neutron scattering study of the $YBa_2Cu_3O_{6+x}$ system *Physica* C **185–189** 86–92
[41] Mook H A, Yethiraj M, Aeppli G, Mason T E and Armstrong T 1993 Polarized neutron determination of the magnetic excitations in $YBa_2Cu_3O_7$ *Phys. Rev. Lett.* **70** 3490–3
[42] Dai P, Mook H A and Doğan F 1998 Incommensurate magnetic fluctuations in $YBa_2Cu_3O_{6.6}$ *Phys. Rev. Lett.* **80** 1738–41
[43] Fong H F, Bourges P, Sidis Y, Regnault L P, Ivanov A, Gu G D, Koshizuka N and Keimer B 1999 Neutron scattering from magnetic excitations in $Bi_2Sr_2CaCu_2O_{8+\delta}$ *Nature* **398** 588–91
[44] Johnston S, Vernay F, Moritz B, Shen Z-X, Nagaosa N, Zaanen J and Devereaux T P 2010 Systematic study of electron–phonon coupling to oxygen modes across the cuprates *Phys. Rev.* B **82** 064513
[45] Terashima K, Matsui H, Hashimoto D, Sato T, Takahashi T, Ding H, Yamamoto T and Kadowaki K 2006 Impurity effects on electron-mode coupling in high-temperature superconductors *Nature Phys.* **2** 27–31
[46] Falter C 2005 Phonons, electronic charge response and electron–phonon interaction in the high-temperature superconductors *Phys. Status Solidi* b **242** 78–117
[47] Zhang W *et al* 2008 Identification of a new form of electron coupling in the $Bi_2Sr_2CaCu_2O_8$ superconductor by laser-based angle-resolved photoemission spectroscopy *Phys. Rev. Lett.* **100** 107002
[48] Lee W S, Meevasana W, Johnston S, Lu D H, Vishik I M, Moore R G, Eisaki H, Kaneko N, Devereaux T P and Shen Z X 2008 Superconductivity-induced self-energy evolution of the nodal electron of optimally doped $Bi_2Sr_2Ca_{0.92}Y_{0.08}Cu_2O_{8+\delta}$ *Phys. Rev.* B **77** 140504
[49] Schachinger E, Carbotte J P and Timusk T 2009 Characteristics of oxygen isotope substitutions in the quasiparticle spectrum of $Bi_2Sr_2CaCu_2O_{8+\delta}$ *Europhys. Lett.* **86** 67003
[50] Nazarenko A and Dagotto E 1996 Possible phononic mechanism for $d_{x^2-y^2}$ superconductivity in the presence of short-range antiferromagnetic correlations *Phys. Rev.* B **53** R2987–90
[51] Normand B, Kohno H and Fukuyama H 1996 Spin-phonon coupling in the single-layer extended t–J model *Phys. Rev.* B **53** 856–70
[52] Nunner T S, Schmalian J and Bennemann K H 1999 Influence of electron–phonon interaction on spin-fluctuation-induced superconductivity *Phys. Rev.* B **59** 8859–68
[53] Rameau J D, Yang H-B, Gu G D and Johnson P D 2009 Coupling of low-energy electrons in the optimally doped $Bi_2Sr_2CaCu_2O_{8+\delta}$ superconductor to an optical phonon mode *Phys. Rev.* B **80** 184513

[54] Vishik I M *et al* 2010 Doping-dependent nodal fermi velocity of the high-temperature superconductor $Bi_2Sr_2CaCu_2O_{8+\delta}$ revealed using high-resolution angle-resolved photoemission spectroscopy *Phys. Rev. Lett.* **104** 207002

[55] Anzai H *et al* 2010 Energy-dependent enhancement of the electron-coupling spectrum of the underdoped $Bi_2Sr_2CaCu_2O_{8+\delta}$ superconductor *Phys. Rev. Lett.* **105** 227002

[56] Johnston S, Vishik I M, Lee W S, Schmitt F, Uchida S, Fujita K, Ishida S, Nagaosa N, Shen Z X and Devereaux T P 2012 Evidence for the importance of extended Coulomb interactions and forward scattering in cuprate superconductors *Phys. Rev. Lett.* **108** 166404

[57] He J *et al* 2013 Coexistence of two sharp-mode couplings and their unusual momentum dependence in the superconducting state of $Bi_2Sr_2CaCu_2O_{8+\delta}$ revealed by laser-based angle-resolved photoemission *Phys. Rev. Lett.* **111** 107005